I. Troch, F. Breitenecker, eds. ISBN 978-3-901608-35-3

MODEL ORDER REDUCTION FOR MULTIPLE GEOMETRIC PARAMETERS

O. Farle, M. Lösch, R. Dyczij-Edlinger
Saarland University, Germany

Corresponding author: O. Farle, Laboratory for Electromagnetic Theory, Dept. of Physics and Mechatronics
Saarland University, D-66123 Saarbrücken, Germany, o.farle@lte.uni-saarland.de

Abstract.

This paper describes an order-reduction method for finite-element models with multiple geometrical parameters. In this context, the main challenge is to handle parameter-dependencies that are given by rational functions of complicated structure. The proposed methodology consists of two major steps: it first constructs an interpolated model and then applies a robust model-order reduction algorithm for multivariate polynomial parameter-dependence. We present the theory of the suggested approach and demonstrate its practical usefulness by numerical examples taken from computational electromagnetics.

1 Introduction

While the finite element (FE) method is a well-established tool for the numerical analysis of linear mechanical or electromagnetic systems, its applicability to structures featuring free parameters, such as in response surface modeling, shape optimization, or inverse problems, is still limited by the large amount of computer runtime needed for factorizing large-scale FE matrices repeatedly. In such applications, methods of model-order reduction (MOR) provide a very attractive alternative to full FE analysis, because the resulting reduced-order models (ROMs) are of small dimensions and inexpensive to analyze. In view of the large scales of typical FE systems, single-point MOR methods are particularly efficient, because they need to factorize the original matrix at one expansion point only. Single-point algorithms for multiple parameters can be found in [1] – [6] . However, the ones are limited to small parameter domains due to numerical issues [1] – [4], and the others to multi-linear parameter-dependence [5] [6]. In a recent publication [7], we proposed a new approach that is not only numerically robust but also handles polynomial parameterization.

The main difficulty with geometrical parameters is that they enter the FE systems in the form of complicated multivariate rational functions. Hence the MOR methods stated above do not apply. Moreover, constructing such functions explicitly may be very tedious or even impossible in real-world applications, because it requires to track functional dependencies on possibly multiple geometric parameters from the solid modeler through the mesh generator all the way to the final FE system. For these reasons, we propose to replace the original functional dependencies by suitable polynomial interpolations: it suffices to instantiate the FE model at discrete points in parameter space, and the resulting system is accessible to the MOR method of [7].

In the following, we first outline the fundamentals of multivariate MOR for polynomial parameterization, then turn to the specifics of the proposed method for geometric parameterization, and close with two numerical examples.

2 Polynomial Parameter-Dependence

In the following, we just treat the single-input-single-output case. Consider a system of linear equations of dimension n, which is parameterized by a polynomial of order M in N scalar variables, $\mathbf{s} = (s_1, \ldots, s_N)$, and a scalar-valued transfer function $H(\mathbf{s})$. Using multi-index notation, we have

$$\Big(\sum_{|\alpha|<M} \mathbf{s}^\alpha \mathbf{A}_\alpha\Big)\mathbf{x} = \Big(\sum_{|\alpha|<M} \mathbf{s}^\alpha \mathbf{b}_\alpha\Big)u, \tag{1a}$$

$$y = \mathbf{c}^* \mathbf{x}, \tag{1b}$$

$$H(\mathbf{s}) = \mathbf{c}^* \Big(\sum_{|\alpha|<M} \mathbf{s}^\alpha \mathbf{A}_\alpha\Big)^{-1} \sum_{|\alpha|<M} \mathbf{s}^\alpha \mathbf{b}_\alpha. \tag{1c}$$

By defining two matrices $\mathbf{V} \in \mathbb{C}^{n\times m}$ and $\mathbf{W} \in \mathbb{C}^{n\times m}$, with $m \ll n$, we obtain a projection-based ROM, the vectors $\hat{\mathbf{b}}$, $\hat{\mathbf{x}}$, $\hat{\mathbf{c}}$, matrices $\hat{\mathbf{A}}_\alpha$, and transfer function $\hat{H}$ of which are given by

$$\hat{\mathbf{x}}(\mathbf{s}) = \mathbf{V}\mathbf{z}(\mathbf{s}), \tag{2a}$$

$$\hat{\mathbf{b}}_\alpha = \mathbf{W}^* \mathbf{b}_\alpha, \tag{2b}$$

$$\hat{\mathbf{A}}_\alpha = \mathbf{W}^* \mathbf{A}_\alpha \mathbf{V}, \tag{2c}$$

$$\hat{\mathbf{c}}^* = \mathbf{c}^* \mathbf{V}, \tag{2d}$$

$$\hat{H}(\mathbf{s}) = \hat{\mathbf{c}}^* \Big(\sum_{|\alpha|<M} \mathbf{s}^\alpha \hat{\mathbf{A}}_\alpha\Big)^{-1} \sum_{|\alpha|<M} \mathbf{s}^\alpha \hat{\mathbf{b}}_\alpha. \tag{2e}$$

We denote by $\mathbf{z}(\mathbf{s})$ the solution of the following linear system of equations

$$\Big(\sum_{|\alpha|<M} \mathbf{s}^{\alpha}\hat{\mathbf{A}}_{\alpha}\Big)\mathbf{z} = \sum_{|\alpha|<M} \mathbf{s}^{\alpha}\hat{\mathbf{b}}_{\alpha}. \tag{3}$$

The error in the ROM depends critically on the choice of trial and test spaces colsp$\mathbf{V}$ and colsp$\mathbf{W}$. The two prototypes for constructing $\mathbf{V}$ and $\mathbf{W}$ are given by single-point methods, which match all moments up to order Q of the transfer function $H(\mathbf{s})$ about a single expansion point $\mathbf{s}_0$,

$$\frac{\partial^{|q|}\hat{H}}{\partial \mathbf{s}^q}\Big|_{\mathbf{s}_0} = \frac{\partial^{|q|}H}{\partial \mathbf{s}^q}\Big|_{\mathbf{s}_0} \qquad \text{for } |q| < Q, \tag{4}$$

and multi-point methods, which match the original solution $\mathbf{x}(\mathbf{s})$ at P interpolation points $\mathbf{s}_p$,

$$\hat{\mathbf{x}}(\mathbf{s}_p) = \mathbf{x}(\mathbf{s}_p) \qquad \text{for } p = 1 \ldots P. \tag{5}$$

While multi-point methods are generally more robust, the advantage of single-point methods is speed: once a factorization of the FE matrix at the expansion point is available, a sequence of inexpensive forward-back substitutions suffices to generate the entire ROM.

2.1 Trial and Test Spaces for the Single-Point Algorithm

We restrict ourselves to $u = 1$ and quadratic dependence on two parameters s_1 and s_2,

$$\left(\mathbf{A}_{00}+s_1\mathbf{A}_{10}+s_2\mathbf{A}_{01}+s_1^2\mathbf{A}_{20}+s_1s_2\mathbf{A}_{11}+s_2^2\mathbf{A}_{02}\right)\mathbf{x} = \left(\mathbf{b}_{00}+\ldots+s_2^2\mathbf{b}_{02}\right), \tag{6}$$

with $\mathbf{A}_{00}$ being invertible. By expanding the solution $\mathbf{x}$ of (6) in a Taylor series,

$$\left(\mathbf{A}_{00}+s_1\mathbf{A}_{10}+\ldots+s_2^2\mathbf{A}_{02}\right)\Big(\sum_{e=0}^{\infty}\sum_{i=0}^{e} s_1^i s_2^{e-i}\mathbf{x}_{i,e-i}\Big) = \mathbf{b}_{00}+s_1\mathbf{b}_{10}+\ldots+s_2^2\mathbf{b}_{02}. \tag{7}$$

and comparing coefficients, we obtain the recursion

$$\begin{aligned}
\mathbf{x}_{00} &= \mathbf{A}_{00}^{-1}\mathbf{b}_{00}\\
\mathbf{x}_{10} &= \mathbf{A}_{00}^{-1}\left(\mathbf{b}_{10}-\mathbf{A}_{10}\mathbf{x}_{00}\right)\\
&\vdots\\
\mathbf{x}_{30} &= \mathbf{A}_{00}^{-1}\left(-\mathbf{A}_{10}\mathbf{x}_{20}-\mathbf{A}_{20}\mathbf{x}_{10}\right)\\
&\vdots\\
\mathbf{x}_{ij} &= \mathbf{A}_{00}^{-1}\left(-\mathbf{A}_{10}\mathbf{x}_{i-1,j}-\mathbf{A}_{01}\mathbf{x}_{i,j-1}-\mathbf{A}_{20}\mathbf{x}_{i-2,j}-\mathbf{A}_{11}\mathbf{x}_{i-1,j-1}-\mathbf{A}_{02}\mathbf{x}_{i,j-2}\right),
\end{aligned} \tag{8}$$

which defines the *multivariate Krylov space of order two* $\mathscr{K}_q\left(\mathbf{A}_{00}^{-1}\mathbf{A}_{kl}, \mathbf{A}_{00}^{-1}\mathbf{b}_{kl}\right)$:

$$\mathscr{K}_q\left(\mathbf{A}_{00}^{-1}\mathbf{A}_{kl}, \mathbf{A}_{00}^{-1}\mathbf{b}_{kl}\right) = \mathrm{span}\{\mathbf{x}_{ij} \,|\, i+j \le q\}, \tag{9}$$

i.e., a parameter-independent subspace spanned by all $\mathbf{x}_{ij}$ with $i+j \le q$, Hence, when $\mathbf{V}$ is chosen such that

$$\mathrm{colsp}\mathbf{V} = \mathscr{K}_q\left(\mathbf{A}_{00}^{-1}\mathbf{A}_{kl}, \mathbf{A}_{00}^{-1}\mathbf{b}_{kl}\right), \tag{10}$$

the reduced transfer function $\hat{H}$ will possess the moment-matching property (4). A rigorous proof is by induction. A similar derivation shows that the number of matching moments increases to $2q+1$, when $\mathbf{W}$ is taken such that

$$\mathrm{colsp}\mathbf{W} = \mathscr{K}_q\left(\mathbf{A}_{00}^{*-1}\mathbf{A}_{kl}^{*}, \mathbf{A}_{00}^{*-1}\mathbf{c}_{kl}\right), \tag{11}$$

$$\mathbf{c}_{kl} = \begin{cases} \mathbf{c} & \text{for } (k,l) = (0,0),\\ \mathbf{0} & \text{else.} \end{cases} \tag{12}$$

For improved numerical robustness, our actual algorithm does not implement the recursion (8) directly. Rather, we employ orthogonal bases for the Krylov spaces (9) and (11). See [7] for details.

3 Geometric Parameters in the Finite Element Method

To illustrate the complicated nature of the dependency of the FE matrices on geometric parameters, let us start from a single finite element. While the associated element matrices are invariant under the six rigid body transformations, their dependencies on the remaining degrees of freedom are given by rational functions. Specifically, when the element size h is rescaled, the mass matrix $\mathbf{T}_{el}$ changes proportionally to h, whereas the variation of the stiffness matrix $\mathbf{S}_{el}$ is proportional to $1/h$. In case of general deformations, rational functions of even higher order emerge. Since the global FE matrices are computed by summing up all element contributions, their entries end up to be multivariate rational functions of high order. In consequence, we face the following complications:

- Since the MOR method of Section 2 requires all parameter-dependencies to be smooth, topological changes in the mesh are not permissible. Hence all parameter variations must be small enough so that the corresponding FE meshes can be derived from a nominal discretization by continuous deformation. Otherwise one has to resort to meta-modelling techniques [9] [10]. Note that such techniques may still utilize the proposed MOR approach as a fast subdomain solver.
- The MOR method of Section 2 requires polynomial parameter-dependence, whereas the FE matrices are of rational type. Since denominators are entry-specific and of high degree, multiplication by the smallest common multiple is not an option.
- Finally, the construction of parameter-dependent FE matrices and right-hand-side (RHS) vectors requires all parametric information to propagate from the solid model through the meshing process to the core of the FE solver. Rigorous construction, especially in case of multiple parameters, requires tools like automatic differentiation or symbolic algebra, which may not be viable for complicated real-world problems.

3.1 Proposed Method

In view of the arguments above, we have to cope with the fact that explicit parameter dependence at the FE level may generally not be available. Therefore, we suggest to take a more direct but approximate approach:

1. Mesh parameterization. Given a nominal mesh $\mathscr{M}_0$ at the expansion point, we construct a parametric mesh $\mathscr{M}(\mathbf{s})$ with the following properties:
   (a) The node positions of $\mathscr{M}(\mathbf{s})$ are smooth functions of parameters $\mathbf{s}$.
   (b) $\mathscr{M}(\mathbf{s})$ is topologically equivalent to $\mathscr{M}_0$.
   (c) $\mathscr{M}(\mathbf{s})$ is a valid FE mesh over the entire parameter domain.
2. Interpolation. We interpolate the parameter-dependency of the FE system by multivariate polynomials of low order $p_\beta(\mathbf{s})$ [11]. For this purpose, we instantiate the mesh at a unisolvent set of sampling points $\mathbf{s}_\beta$ in parameter space, at which we assemble the global FE matrix $\mathbf{A}(\mathbf{s}_\beta)$ and the RHS vector $\mathbf{b}(\mathbf{s}_\beta)$. The resulting interpolations $\tilde{\mathbf{A}}(\mathbf{s})$ and $\tilde{\mathbf{b}}(\mathbf{s})$ are given by
$$\tilde{\mathbf{A}}(\mathbf{s}) = \sum_\beta p_\beta(\mathbf{s})\mathbf{S}(\mathbf{s}_\beta), \tag{13a}$$
$$\tilde{\mathbf{b}}(\mathbf{s}) = \sum_\beta p_\beta(\mathbf{s})\mathbf{b}(\mathbf{s}_\beta), \tag{13b}$$
   and the approximate system features polynomial parameterization (1c), as required. Note that we interpolate the various stiffness and mass matrices separately.
3. MOR for polynomial parameter-dependence. See Section 2.

The major advantage of our strategy is that parameterization is kept away from low-level FE computations, and that multivariate rational functions are never handled explicitly. The obvious disadvantage is its approximate nature. Each stage of our method is associated with a specific kind of error. Specifically, we have:

- *Mesh deformation error:* Large changes in geometry lead to large mesh deformations, which in turn may result in poor mesh quality, as illustrated in Fig. 2. The latter may negatively affect the approximation properties of the FE model. In addition, the FE mesh may become too coarse in some critical regions.
- *Interpolation error:* In between sampling points, the interpolated system
$$\tilde{\mathbf{A}}(\mathbf{s})\tilde{\mathbf{x}}(\mathbf{s}) = \tilde{\mathbf{b}}(\mathbf{s}) \tag{14}$$
  does not coincide with the original one,
$$\mathbf{A}(\mathbf{s})\mathbf{x}(\mathbf{s}) = \mathbf{b}(\mathbf{s}). \tag{15}$$
  Therefore, the resulting transfer functions, $\tilde{H}(\mathbf{s})$ and $H(\mathbf{s})$, differ. The quality of (14) depends not only on the degree of the interpolation polynomial but also the choice of sampling points.
- *MOR error:* This is the error committed by approximating the interpolated system (14) by the ROM (2).

4 Numerical Examples

4.1 Waveguide Iris

The main purpose of our first example is to compare different interpolation schemes and to quantify the errors associated with each stage of approximation. We consider a metal iris of zero thickness within a rectangular waveguide with $\mu_r = \varepsilon_r = 1$. As indicated by Fig. 1, just one quarter of the structure has been modeled. We compute the reflection coefficient S_{11} as a function of the width a and the height b of the opening, as well as the

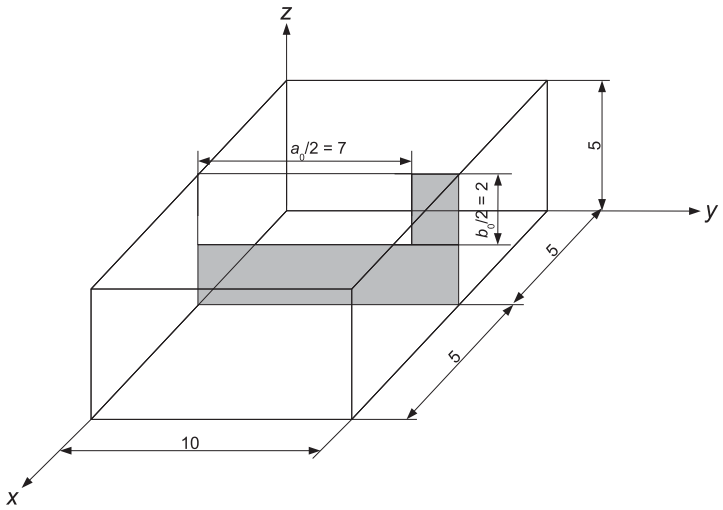

Figure 1: One quarter of the waveguide iris. Dimensions are in mm.

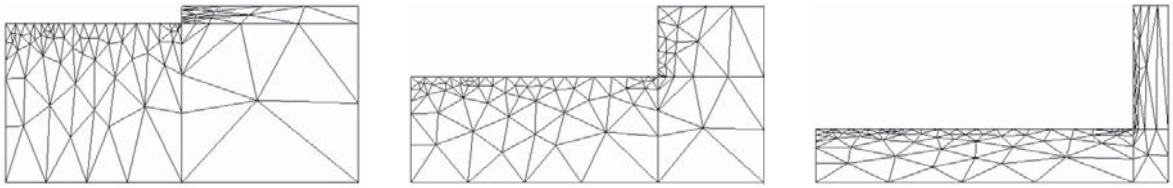

(a) $a = 10$, $b = 1$. (b) $a = 14$, $b = 4$. (c) $a = 18$, $b = 7$.

Figure 2: Surface mesh of one quarter of the waveguide iris for different parameter values. Dimensions are in mm.

operating frequency f in the range

$$a = 10 \ldots 18\,\text{mm}, \qquad b = 1 \ldots 7\,\text{mm}, \qquad f = 8 \ldots 17\,\text{GHz}. \tag{16}$$

Note that the variations in geometry are very large. Even though modes of higher order are propagable at some frequencies, structural symmetry prevents such waveforms from being excited. The expansion point is set at (a_0 = 14 mm, $b_0 = 4$ mm, $f = 10$ GHz), and FE discretization results in a total of 41454 second order degrees of freedom.

In our prototype implementation, the mesh is parameterized by displacing nodal positions with the help of simple, problem-specific functions, which are constructed in such a way that deformation decreases linearly in the direction from the iris to the outer boundary. Fig. 2(b) presents the nominal FE mesh at the expansion point, and Figs. 2(a) and 2(c) show extreme instantiations at two opposite points on the outer boundary of the parameter domain.

Our first test compares full FE solutions based on deformed meshes and adaptive remeshing, for approximately the same number of unknowns. Fig. 3(a) shows results for $|S_{11}|$, and Fig. 3(b) presents the error in S_{11} for the deformed mesh with respect to adaptive remeshing. The maximum error is in the order of $4 \cdot 10^{-3}$. It is mainly caused by poor mesh quality resulting from large deformations; see Figs. 2(a) and 2(c). A two-dimensional cut through the response hypersurface at $f = 10\,\text{GHz}$ using deformed meshes is given in Fig. 4.

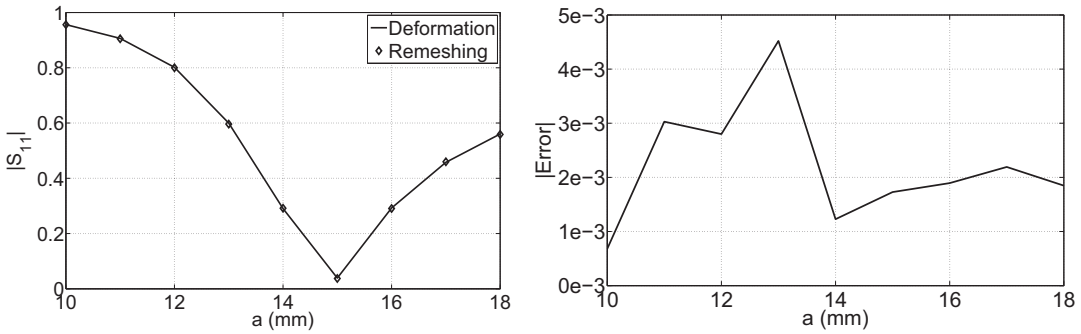

(a) $|S_{11}|$ (b) |Error in S_{11}|

Figure 3: Comparison of $|S_{11}|$ for full FE solutions based on deformed mesh and adaptive remeshing. Parameters: $b = 1\,\text{mm}$ and $f = 10\,\text{GHz}$.

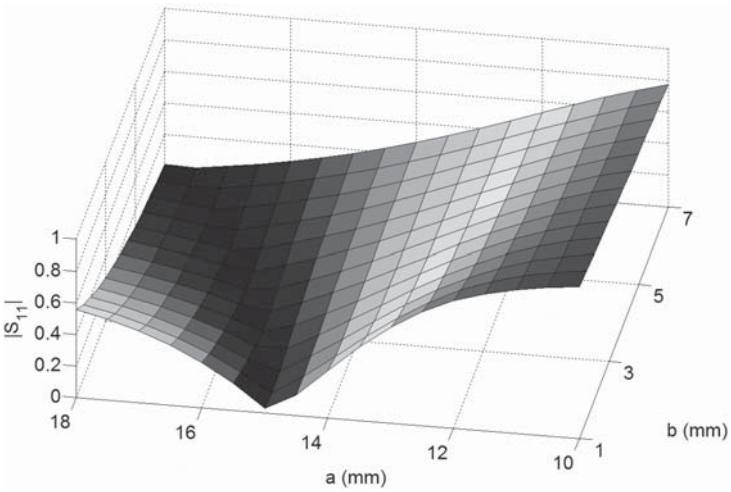

Figure 4: $|S_{11}|$ as function of width a and height b with deformed mesh at $f = 10$ GHz.

Table 1: Computational Data for Iris[1].

	6^{th} order ROM	8^{th} order ROM	Full FE
Dimension	168	330	78448
Interpolation[2] (s)	781.7	781.7	N.A.
Generation (s)	1973.8	3890.6	N.A.
Solution (s)	0.0277	0.125	42.47
Evaluations per s	36.1	7.99	0.0235

[1] MATLAB implementation on AMD Opteron 246 processor, 1.99GHz.

[2] 5×7 Chebyshev points.

We next examine different interpolation schemes to achieve polynomial parameter dependence. For this purpose, we compare FE solutions based on the interpolated model (14) and instantiations of the parametric mesh, respectively. Figs. 5, 6, and 7 present the locations of 5×7 equidistant interpolation points, of 6^{th} order serendipity points after [12], and of 5×7 Chebyshev points, i.e., the tensor product of the zeros of the Chebyshev polynomial of order $n+1$, as well as the corresponding error surfaces for S_{11} at $f = 10$ GHz. Overall, errors are in the order of 10^{-3}. While equidistant and serendipity interpolation lead to very similar results, the errors due to the Chebyshev scheme are significantly smaller and spread out more evenly over the parameter domain.

Our final test aims at quantifying the error committed at the MOR stage. For this purpose, we start from the polynomially parameterized model obtained from the Chebyshev interpolation points of Fig. 7 and compute two ROMs of order 6 and 8, respectively, for the three parameters a, b, and f. Fig. 8(a) shows the frequency response for ($a = 17$ mm, $b = 6$ mm), and Fig. 8(b) gives the corresponding errors. It can be seen that ROM errors are in the order of 10^{-5} and 10^{-7}, respectively, over the entire frequency range, whereas the dominant error contributions stem from the matrix interpolation stage and are in the order of 10^{-3}.

Table 1 presents the CPU times for building the polynomially parameterized system and the subsequent MOR process, respectively. It can be seen that overall runtimes are dominated by the MOR step. For comparison, we have also included computational data for a full FE simulation. The immense speedup attainable by MOR is made clear by the runtimes and solution rates given in the last two rows of Table 1. A single FE solution takes 42 s, whereas just 0.03 s are required to evaluate the 6^{th} order ROM. All computations were performed on an AMD Opteron 246 processor.

4.2 Bandpass Filter

Fig. 9 presents a bandpass filter consisting of three metal rods within an empty rectangular waveguide. We consider four model parameters: the diameters of the rods, d_1 and d_2, their distance l_{12}, and the operating frequency f. A rough hand calculation for a center frequency of 1.1 GHz and a passband return loss of 10 dB yields the expansion point($d_1 = 16$ mm, $d_2 = 40$ mm, $l_{12} = 180$ mm, $f = 1.1$ GHz). To accommodate large variations in all model parameters, we define the parameter domain by

$$d_1 = 9 \ldots 30 \text{ mm}, \qquad l_{12} = 150 \ldots 210 \text{ mm}, \qquad d_2 = 23 \ldots 74 \text{ mm}, \qquad f = 0.8 \ldots 1.4 \text{ GHz}. \tag{17}$$

Using the proposed MOR methodology, a single FE solution for the nominal design is sufficient to generate a whole family of 20 dB bandpass filters of greatly varying bandwidth BW and center frequency f_c. The ROM employs a tensor-product grid of $7 \times 7 \times 7$ Chebyshev points to interpolate the dependence of the FE matrices on the three geometrical parameters. Table 2 summarizes the parameter values and bandwidths of selected filter configurations

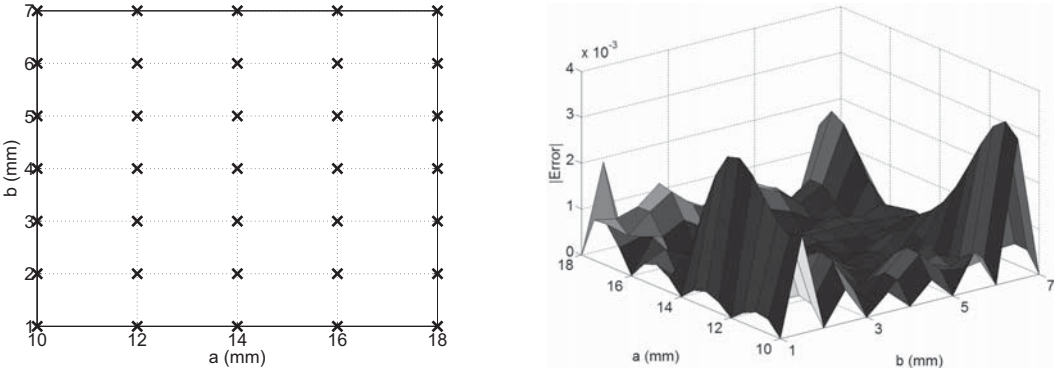

Figure 5: Interpolation by 5×7 equidistant and resulting interpolation error in S_{11} at $f = 10$ GHz.

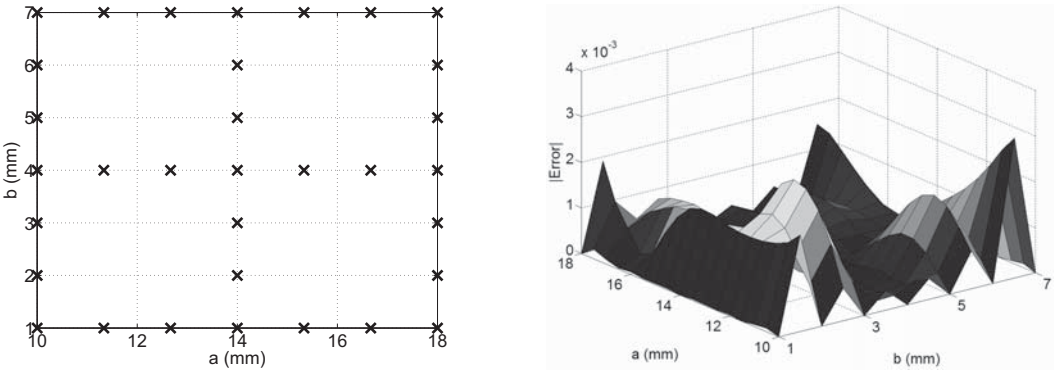

Figure 6: Interpolation by 6^{th} order serendipity points and resulting interpolation error in S_{11} at $f = 10$ GHz.

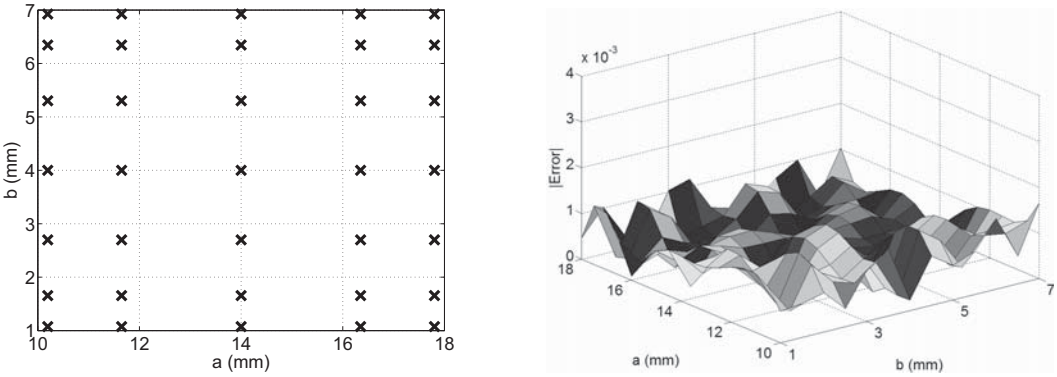

Figure 7: Interpolation by 5×7 Chebyshev points and resulting interpolation error in S_{11} at $f = 10$ GHz.

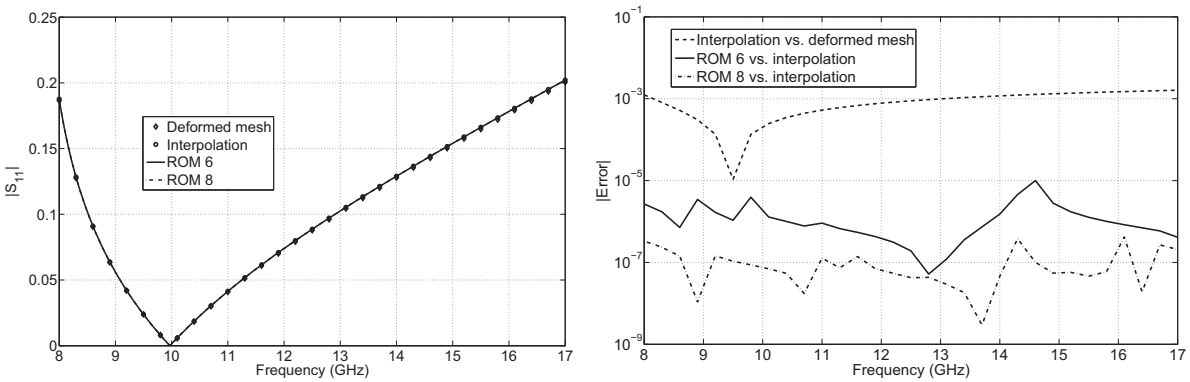

(a) Magnitude of S_{11}. (b) Magnitude of error in S_{11}.

Figure 8: Frequency response of waveguide iris and associated errors for $a = 17\,\text{mm}$, $b = 6\,\text{mm}$.

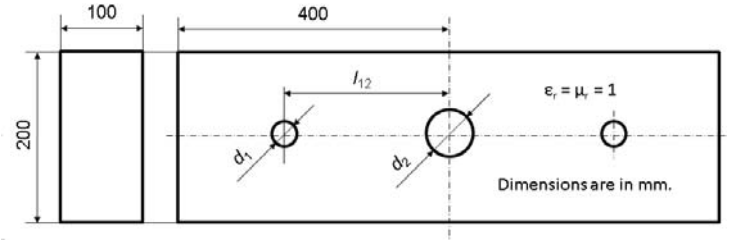

Figure 9: Structure of bandpass filter.

Table 2: Selected Filter Configurations*

f_c (GHz)	BW (MHz)	d_1 (mm)	d_2 (mm)	l_{21} (mm)
1.00	16.5	9.0	29.15	205.00
1.10	3.4	30.0	63.30	206.00
1.10	14.9	16.0	40.40	180.10
1.10	31.5	9.0	27.15	163.40
1.20	6.4	14.9	36.77	150.00
1.20	28.2	30.0	61.00	177.72
1.30	15.8	26.0	53.80	150.19
1.34	13.1	30.0	58.43	150.00

* Passband return loss: 20 dB max. Circular cross-sections are modelled by regular 16-gons of outer diameter d_i.

with center frequencies from 1.0 to 1.34 GHz. Fig. 10 and Fig. 11 present the corresponding frequency responses and errors of a 5^{th} order ROM compared to full FE solutions at 201 equidistant frequency points. Even though the changes in filter geometry are very significant, errors in S_{11} are typically in the order of 10^{-4} to 10^{-3}. Table 3 gives computational data and runtimes for the full FE system and ROMs of order 4 and 5, respectively. Even for the more expensive 5^{th} order ROM, the speedup for a single solution is 324! Even better, by diagonalizing the ROM matrices, we are able to compute a whole frequency sweep of 2001 sampling points in 1.4 s on an Opteron 250 processor, including the time for the eigenvalue decomposition. For comparison, 2001 FE solutions take 8229.5 s.

5 Summary and Outlook

We have presented an interpolation technique that extends the scope of MOR methods for polynomial parameter dependence to geometry variations. The resulting ROMs are fast to evaluate and provide similar levels of accuracy as the original FE systems. Future applications will include shape optimization and inverse problems.

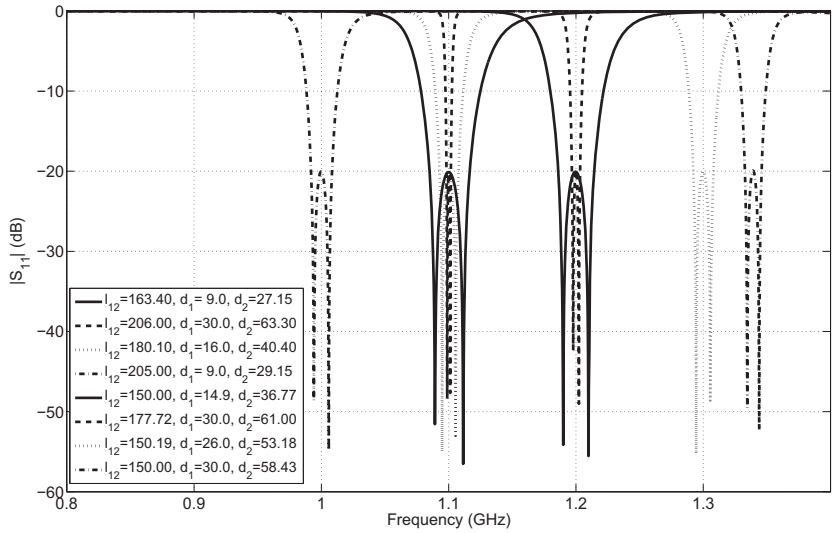

Figure 10: Magnitude of S_{11} versus frequency for selected filter configurations and a 5^{th} order ROM.

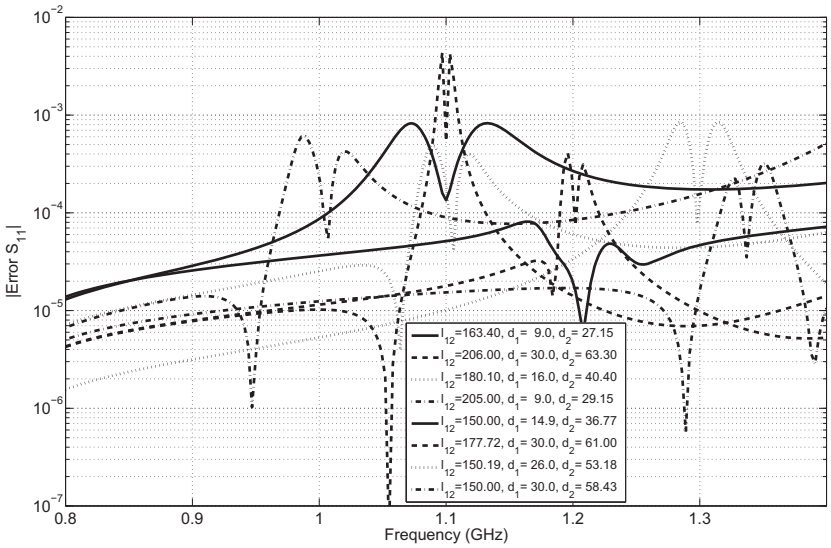

Figure 11: Error in S_{11} versus frequency w.r.t. full FE solutions for selected filter configurations and a 5^{th} order ROM.

Table 3: Computational Data for Filter[1].

	4^{th} order ROM	5^{th} order ROM	Full FE
Dimension	140	252	44346
Interpolation[2] (s)	5388.5	5388.5	N.A.
Generation (s)	6241.0	8049.4	N.A.
Single solution (s)	3.491e-3	1.271e-2	4.1127
Freq. sweep[3] (s)	0.4536	1.402	8229.5

[1] MATLAB implentation on AMD Opteron 250 processor, 2.39 GHz.

[2] $7 \times 7 \times 7$ Chebyshev points.

[3] Frequency sweep of 2001 sampling points.

6 References

[1] P. Gunupudi, R. Khazaka, and M. Nakhla, "Analysis of transmission line circuits using multidimensional model reduction techniques," *IEEE Trans. Adv. Packaging,* vol. 25, no. 2, pp. 174-180, 2002.

[2] D.S. Weile, E. Michielssen, E. Grimme, and K. Gallivan, "A method for generating rational interpolant reduced order models of two-parameter linear systems", *Applied Mathematics Letters,* vol. 12, pp. 93-102, July 1999.

[3] D.S. Weile, E. Michielssen, "Analysis of frequency selective surfaces using two-parameter generalized rational Krylov model-order reduction", *IEEE Trans. Antennas Propagat.,* vol. 49, pp. 1539-1549, Nov. 2001.

[4] L. Daniel, C.S. Ong, L.S. Chay, K.H. Lee, J. White, "A Multiparameter Moment-Matching Model-Reduction Approach for Generating Geometrically Parameterized Interconnect Performance Models", *IEEE Trans. Comp.-Aided Design Integrated Circuits,* vol. 23, pp. 678-693, May 2004.

[5] L. Codecasa, "A novel approach for generating boundary condition independent compact dynamic thermal networks of packages, *IEEE Trans. Compononents Packaging*, vol. 28, pp. 593-604, Dec. 2005.

[6] Y.-T. Li, Z. Bai, Y. Su, Z. Zeng, "Model Order Reduction of Parameterized Interconnect Networks via a Two-Directional Arnoldi Process," IEEE Trans. Comp.-Aided Design Integrated Circuits, vol. 27, no. 9, pp. 1571-1582, Sep. 2008.

[7] O. Farle, V. Hill, P. Ingelström, R. Dyczij-Edlinger, "Multi-Parameter Polynomial Order Reduction of Linear Finite Element Models," *Mathematical and Computer Modelling of Dynamical Systems*, vol. 14, no. 5, pp. 421-434, Oct. 2008.

[8] M.A. González de Aza, J.A. Encinar, J. Zapata, and M. Lambae, "Full-wave analysis of cavity-backed and probe-fed microstrip patch arrays by a hybrid mode-matching generalized scattering matrix and finite-element method," *IEEE Trans. Antennas Propagat.,* vol. 46, pp. 234-242, 1998.

[9] A. H. Zaabab, Q. J. Zhang, and M. Nakhla, "A Neural Network Modeling Approach to Circuit Optimization and Statistical Design," *IEEE Trans. Microwave Theory Tech.*, vol. 43, no. 6, pp. 1349 - 1358, June 1995.

[10] D. Deschrijver, T. Dhaene, and D. De Zutter, "Robust Parametric Macromodeling Using Multivariate Orthonormal Vector Fitting," *IEEE Trans. Microwave Theory Tech.*, vol. 56, no. 7, pp. 1661 - 1667, July 2008.

[11] P.J. Davis, Interpolation and Approximation, New York: Dover Publ., 1975, pp. 24 - 94.

[12] W.J. Gordon and C.A. Hall, "Transfinite element methods: blending-function interpolation over arbitrary curved element domains," *Numer. Math.*, vol. 21, pp. 109-129, 1973.